Zeolites

DOI: 10.1002/ange.201306370

Intergrowth Structure and Aluminium Zoning of a Zeolite ZSM-5 Crystal as Resolved by Synchrotron-Based Micro X-Ray Diffraction Imaging**

*Zoran Ristanović, Jan P. Hofmann, Upakul Deka, Tobias U. Schülli, Marcus Rohnke, Andrew M. Beale, and Bert M. Weckhuysen**

Zeolites represent an important group of heterogeneous catalysts and are heavily used in the petrochemical and refining industries.[1] Since their discovery, zeolites with MFI topology, namely ZSM-5, have been utilized in a number of large-scale industrial applications. The unique combination of acidic properties and pore architecture[2] enabled their use as solid acid catalysts in the alkylation of arenes,[3] the oligomerization of light olefins,[4] and the methanol-to-hydrocarbon reaction.[5] The internal crystallographic architecture, micro- and mesoporosity, as well as the 3D distribution of Brønsted acid sites play a crucial role in the catalytic performance of zeolites.[6]

To better understand the chemistry of these industrially important catalytic materials, large coffin-shaped zeolite ZSM-5 crystals have been extensively investigated as model systems. This has been accomplished by making use of a wide variety of microscopic and spectroscopic methods. One of the intriguing discussions is related to the precise 3D structure of the zeolite intergrowth,[7] which consists of at least six individual subunits,[7e] and its impact on the diffusion and reactivity of a wide range of probe molecules, such as furfuryl alcohol, thiophene, and styrene derivatives.[8] Numerous techniques were applied to visualize the structure and chemistry of these crystals, including interference,[9] UV/Vis, and fluorescence microscopy,[10] coherent anti-Stokes Raman scattering spectromicroscopy,[11] synchrotron IR microscopy,[12] and electron backscatter diffraction (EBSD) combined with focused ion beam (FIB) milling.[7c,d]

However, none of the above-mentioned characterization studies provided non-invasive 3D crystallographic information of the whole zeolite crystal. For example, optical microscopy techniques, such as UV/Vis, confocal fluorescence, and IR micro-spectroscopy, only gather indirect structural information through a detailed analysis of the location and orientation of specific probe molecules within the porous framework. Furthermore, as zeolites are poor electron scatterers, the direct invasive, but time-consuming FIB-EBSD approach may even lead to a complete amorphization of the probed crystalline material. In addition, the FIB-EBSD method suffers from difficulties with the interpretation of the inherently weak electron backscatter diffraction patterns.[13]

The characterization method of choice to unravel the structure and chemical composition of zeolites in great detail is X-ray diffraction (XRD) analysis.[14] However, both powder and conventional single-crystal XRD measurements cannot provide spatially resolved information on, for example, the intergrowth structure and the location of aluminium. Ideally, non-invasive crystallographic information on the micrometer-scale over the whole zeolite crystal is needed. Advances in synchrotron-based X-ray microscopy now provide the methods that enable scientists to use highly focused and brilliant X-rays for the characterization of advanced materials.[15] To date, there has been no X-ray crystallographic study that sheds light on the crystallographic structure of a single zeolite crystal, such as ZSM-5, with high spatial and angular (2θ) resolution. Herein, we report the first micro X-ray diffraction (μXRD) crystallography imaging study of a single zeolite crystal, taking the large coffin-shaped zeolite ZSM-5 crystals ($Si/Al = 17$, $100 \times 20 \times 20\ \mu m^3$) as the model system. More details on the crystallographic structure of the crystals and the chemistry of zeolite ZSM-5 crystals can be found in the Supporting Information and in recent examples in the literature.[16]

The diffraction responses of a single large zeolite ZSM-5 crystal were mapped with a lateral resolution of 2 μm by applying a micro-focused X-ray beam (8.5 keV). After detection of the diffraction peaks of interest, spatially

[*] Z. Ristanović,[+] Dr. J. P. Hofmann,[+] Dr. U. Deka, Dr. A. M. Beale, Prof. Dr. Ir. B. M. Weckhuysen
Inorganic Chemistry and Catalysis
Debye Institute for Nanomaterials Science, Utrecht University
Universiteitsweg 99, 3584 CG Utrecht (The Netherlands)
E-mail: b.m.weckhuysen@uu.nl
Homepage: http://www.anorg.chem.uu.nl
Dr. T. U. Schülli
European Synchrotron Radiation Facility ESRF, beamline ID01
6 rue Jules Horowitz, 38043 Grenoble Cedex (France)
Dr. M. Rohnke
Institute of Physical Chemistry, Justus-Liebig-University Giessen
Heinrich-Buff-Ring 58, 35392 Giessen (Germany)
[+] These authors contributed equally to the work.

[**] Z.R. and J.P.H. thank the Dutch National Research School Combination Catalysis (NRSC-C) for funding. J.P.H. thanks the German Research Foundation (DFG) for a postdoctoral research fellowship (Ho4579/1-1). The ESRF is acknowledged for providing beamtime and staff members of ESRF beamline ID 01, and Zafer Öztürk (Utrecht) is acknowledged for experimental support. Machteld Mertens (ExxonMobil, Machelen, Belgium) is thanked for providing the ZSM-5 samples. We thank Prof. Jürgen Janek (Giessen) for granting access to the TOF-SIMS facilities and Julia Kokesch-Himmelreich (Giessen) for confocal-microscopy height-profiling measurements.

Supporting information for this article is available on the WWW under http://dx.doi.org/10.1002/anie.201306370.

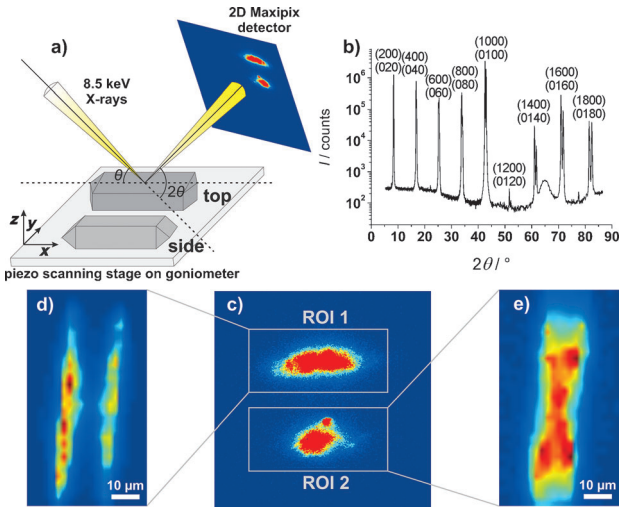

Figure 1. a) Experimental setup; b) θ–2θ XRD scan of a large zeolite ZSM-5 crystal corresponding to (h 0 0) and (0 k 0) Bragg reflections; c) 2D diffraction response of a zeolite ZSM-5 crystal at a fixed θ–2θ diffraction geometry, zoom-in image, resolution: 154 pixels/° (2θ); d, e) diffraction intensity maps of the regions of interest (ROI) 1 and 2.

resolved maps were recorded by moving the crystal with a piezo stage with respect to the X-ray beam, and the responses were detected with a 2D X-ray detector in a fixed geometry. Figure 1 a illustrates the experimental approach. To minimize the footprint of the X-ray beam, higher-order Bragg reflections of (h 0 0) and (0 k 0) lattice planes in the range of $2\theta > 70°$ were used. These reflections clearly show that the splitting for higher diffraction orders is due to small differences in the lattice parameters a and b of ZSM-5 (Figure 1 b). This observation indicates that two different orientations of the crystal lattice (rotated by 90°) are present along the beam trajectory; this fact was subsequently used for the determination of the crystalline phases and the orientation of the intergrowth subunits. Our experimental approach enables the monitoring of changes on very small length scales (bond distances), which provides unprecedented details on the differences of crystallographic parameters along the zeolite ZSM-5 crystal, including information on the 3D distribution of aluminium (see below).

Figure 1 c shows the diffraction response on the 2D X-ray pixel detector for one (x, y) position of the crystal. It is striking that two related reflections of the single zeolite ZSM-5 crystal appear very close in the 2θ space, which makes them ideal candidates for further crystallographic analysis. The two separate peaks are assigned to higher order (16 0 0) and (0 16 0) Bragg reflections of the MFI framework. Their integrated intensity (as defined by ROI1 and ROI2 in Figure 1 c) plotted over the (x, y) piezo movement yields diffraction intensity maps. The lateral distribution of the integrated intensities represents the contribution of a particular crystallographic phase in the zeolite crystal. In this way, diffraction intensity maps with a lateral resolution of 2 µm can be reconstructed for any specific higher-order Bragg reflection. Figure 1 d reveals an hourglass pattern, which is typically observed for ZSM-5 intergrowth by optical micro-spectroscopic techniques,[10a] indicating that the distribution of the (16 0 0) Bragg reflection originates from the pyramidal side subunits. The diffraction response of the remaining four subunits, which are assigned to the closely related (0 16 0) Bragg peak, supports our conclusion that two different crystallographic orientations coexist in the intergrowth structure of large zeolite ZSM-5 crystals (Figure 1 e; for more details on the experimental setup and a definition of regions of interest, see the Supporting Information).

To demonstrate the strength of our experimental approach and to provide more detailed insights into the crystallographic structure of the different subunits of large zeolite ZSM-5 crystals, two crystal orientations with respect to the incident X-ray beam were studied: 1) the orientation denoted as *top* in Figure 2 a, and 2) the orientation denoted as

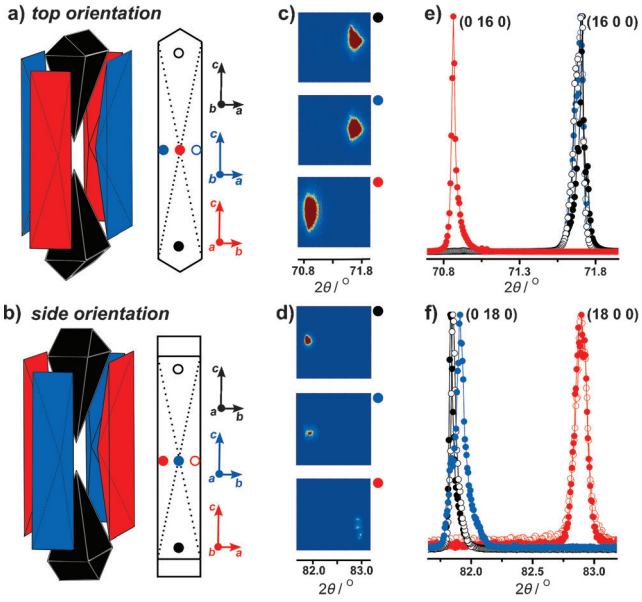

Figure 2. Crystallographic analysis of the intergrowth structure of a single zeolite ZSM-5 crystal. a, b) Zeolite ZSM-5 crystal intergrowth (left) and scheme of the color-coded regions for which the diffraction response was recorded (right) in *top* (a) and *side* (b) orientations. The crystallographic orientation of each subunit is indicated by the color-coded vectors. c, d) Corresponding diffraction patterns on the 2D detector for the color-coded spots; for clarity, the patterns are intentionally rotated by 90°. e, f) Corresponding normalized X-ray diffractograms, presented for fulfilled Bragg conditions of designated reflections.

side in Figure 2 b. To probe the diffraction response of different subunits in these orientations, the diffraction patterns for Bragg incident angles of the beam were recorded from several positions along the crystals (color-coded in Figure 2 a, b). The corresponding detector responses are displayed in Figure 2 c and d and can be translated into a 2θ representation (Figure 2e and f, respectively; for details, see the data treatment section of the Supporting Information). For both orientations of the crystal, two distinct diffraction peaks appear as a result of the intergrowth structure and the orientation of the crystal lattice within the subunits. The contribution of each specific Bragg reflection

will depend on the fraction of the probed subunits in the corresponding crystallographic orientation. The crystal in *top* orientation (Figure 2a,c,e) reveals a diffraction pattern at lower angles that is attributed to top and bottom pyramidal subunits (red), whereas reflections from the remaining four subunits (blue and black) appear shifted by 0.9° in 2θ towards higher angles (lower interplanar d-spacings; Figure 2e). Based on these results, the lattice parameters were calculated to be $a_{ZSM\text{-}5} = 19.92$ Å and $b_{ZSM\text{-}5} = 20.11$ Å, which is in excellent agreement with the values of the corresponding parameters reported for calcined powder ZSM-5 zeolite (monoclinic framework, $a_{ZSM\text{-}5} = 19.879$ Å, $b_{ZSM\text{-}5} = 20.107$ Å).[14] The diffraction intensity corresponding to the (0 16 0) reflection originates from the top and bottom pyramidal subunits, suggesting that straight channels (running along the $b_{ZSM\text{-}5}$ lattice vector) are parallel to the surface of these subunits and the support (red; Figure 2a). The diffraction response assigned to the (16 0 0) reflection is distributed over the side pyramidal subunits (blue) and the closing subunits (black). In these subunits, the $a_{ZSM\text{-}5}$ lattice vector and therefore the sinusoidal channels are oriented parallel to the support, which corresponds to a 90° rotation of the side pyramidal subunits with respect to the top/bottom pyramidal subunits.

When the zeolite ZSM-5 crystal is rotated by 90° along the long crystal axis, which is now referred to as the *side* orientation (Figure 2b), all six subunits are rotated by 90° with respect to the X-ray beam. However, despite the physical rotation of the crystal by 90°, the diffraction response and the relative positions of the diffraction peaks originating from the top/bottom and side pyramidal subunits essentially remain the same. The bulk crystallography can thus be considered as equal for the top/bottom and side pyramidal subunits, which are rotationally congruent. This implies that the porous network is rotated by 90° between the top/bottom and side pyramidal subunits. For the *side* orientation, the diffraction signal from the closing subunits (black; Figure 2b,f) now occurs at lower angles, which finally and unambiguously confirms our working hypothesis on the pore orientation of these subunits: The pore orientation of the closing subunits is now parallel to the pore orientation of the top/bottom pyramidal subunits.

The high lateral resolution and the angular resolving power of 0.007°/pixel provide the possibility to resolve subtle differences between lattice parameters along the crystal bulk. Figure 3a and b present typical (16 0 0) and (0 16 0) diffractograms of a particular (x,y) spot on a zeolite ZSM-5 crystal in the *top* orientation, plotted for different incident angles of the X-ray beam. Close examination of these so-called single (x,y) pixel diffractograms reveals differences in shape and position of the diffraction peaks. This is a result of the scattering geometry, the optical path of the beam, and the crystal structure. Even though only one of the two Bragg reflections is at the specular path for a certain incident angle, the existence of two crystallographically different phases within a single diffraction peak of, for example, the (16 0 0) reflection is evident (Figure 3a). This observation clearly indicates that the interplanar d-spacing of the observed crystallographic planes changes along the crystal. To further

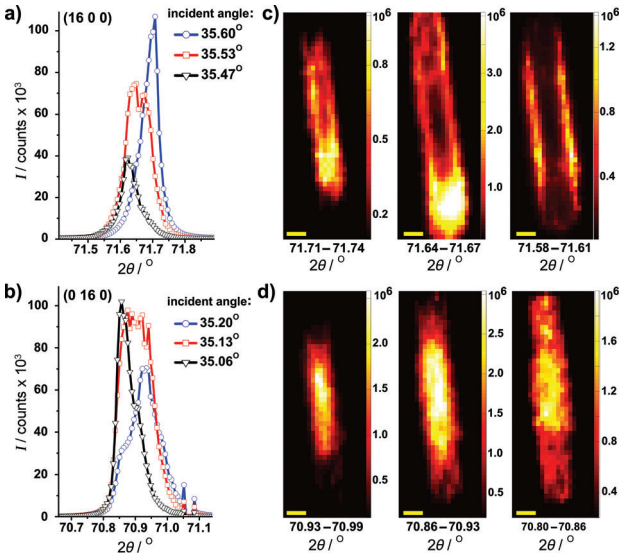

Figure 3. Fine structure of the diffraction peaks and corresponding lateral distribution of the diffraction intensities that result from small changes in the incident diffraction angles. a, b) Reconstructed single (x,y) pixel diffractograms of the (16 0 0) reflection (a) and the (0 16 0) reflection (b) for different incident angles of the beam. c, d) Diffraction intensity maps for different 2θ regions of the (16 0 0) reflection (c) and the (0 16 0) reflection (d). Single (x,y) pixel diffractograms were intentionally chosen to show the complexity of the scattering collected from one spot on the crystal. Diffraction maps are reconstructed for a given 2θ region over all probed incident angles (for more details on the recorded single (x,y) pixel diffractograms, see the Supporting Information). Scale bars: 10 μm.

analyze these features, we reconstructed diffraction intensity maps over relevant 2θ intervals within the (16 0 0) and (0 16 0) reflections (Figure 3c and d).

The resulting diffraction intensity maps reveal zones with different values of lattice parameters along the zeolite ZSM-5 crystal. The expansion of the crystal lattice is evident for both lattice parameters *a* and *b* when moving from the middle towards the edges of the crystal. The trend is more visible in Figure 3c, where the diffraction maps show a core-like region towards lower values of the lattice parameter (here presented as higher 2θ angles), and a 2–3 μm thick rim that indicates a noticeable expansion of the lattice parameter *a* towards higher interplanar spacings. Similar results were obtained for the (0 16 0) reflection, when the intergrowth structure model (Figure 2a) is kept in mind. In this case, top and bottom intergrowth subunits are imaged, and lattice parameters expand from the middle of the crystal towards the surface (Figure 3d), which reflects the pyramidal geometry of the intergrowths at the same time. A similar behavior was noted for all of the studied crystals, including the ones in *side* orientation (for the diffraction maps, see the Supporting Information). The phenomenon of aluminium zoning explains the observed trends. When aluminium is incorporated in the tetrahedral positions of a pure silica parent framework, the crystal lattice expands because of an increased Al–O distance (1.75 Å) as compared to the Si–O distance (1.61 Å).[17] This is demonstrated in Figure 4a, where values of the lattice parameter *a* for the crystal in the *side* orientation are plotted

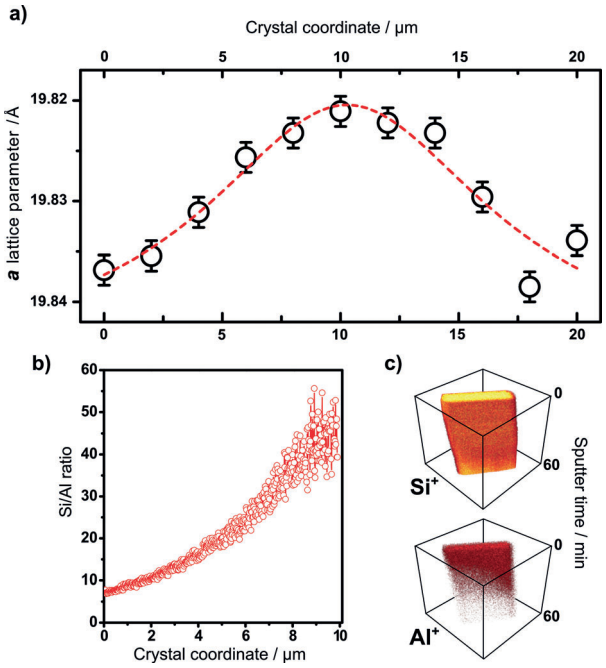

Figure 4. Evidence for the presence of an aluminium gradient along the short crystal axis, as recorded in the *side* orientation. a) Lattice parameter *a* plotted along the short crystal axis; error bars were determined with respect to the size of a single pixel on the 2D detector. b) TOF-SIMS sputter depth profiling of the crystal indicating the estimated Si/Al ratio. c) 3D representation of the depth profiles of Si^+ and Al^+ secondary ions, as a function of sputter time.

against the short crystal coordinate (20 µm). The typical change in the diffraction response is about 0.1° in 2θ, which translates to a change of approximately 0.02 Å in the lattice parameter *a*. Complementary results were obtained for the lattice parameter *b*. This is in line with early crystallographic studies of ZSM-5, where several powders with Si/Al ratios of 70 to 3000 were studied, which reported a maximum change of up to 0.04 Å in the lattice parameter.[12a] It has already been reported that the synthesis of zeolite ZSM-5 starting from the tetrapropylammonium (TPA) template can indeed lead to gradients in aluminium concentration.[18] Our results crystallographically confirm the observed zoning, and provide information on the crystal lattice parameters at the same time. Furthermore, our findings are perfectly in line with electron microprobe experiments on Al zoning by von Ballmoos and Meier, who reported a similar rim structure for the aluminium enrichment of ZSM-5 crystals.[19]

To provide additional insight into the zoning of aluminium, a single zeolite ZSM-5 crystal was subjected to a time-of-flight secondary ion mass spectrometry (TOF-SIMS) sputter-depth profiling analysis. The ion count rates for Si^+ and Al^+ were measured as a function of sputter time (depth). As a rough approximation, the ratio of Si^+/Al^+ can be considered as proportional to the actual Si/Al ratio of the zeolite material (see the Supporting Information). The results are summarized in Figure 4b and c. Figure 4b presents the estimated Si/Al ratio within the zeolite ZSM-5 crystal as a function of increasing sputter depth, and indicates a strong gradient for the aluminium concentration with sputter time. The variation of the Si^+ count rate was less than 10%, whilst the count rate of Al^+ decreased by a factor of 15 on going from the surface of the crystal towards the middle of the crystal (10 µm). The depletion of Al^+ compared to Si^+ is shown in Figure 4c. Sputtering confirms our hypothesis on aluminium zoning, which is also evident from the diffraction maps in Figure 3c and d. One may argue that crystallographic observations on a single zeolite ZSM-5 crystal can be obscured by the existence of an additional phase, more specifically the MEL (ZSM-11) phase, which is a framework topology closely related to MFI (ZSM-5).[7b] However, as explained in the Supporting Information, the 2D XRD analysis of the (h 0 0) and (0 k 0) reflections and the consistency with the lattice parameters of the MFI structure exclude the existence of MEL.

In summary, we have presented a micrometer-resolved X-ray diffraction imaging study to crystallographically substantiate the intergrowth structure model earlier proposed for large coffin-shaped zeolite ZSM-5 crystals and to provide new insights into the differences in crystallographic parameters along the crystal. The bulk crystallography of the pyramidal top, bottom, and side lids was identical, whereas the top and side subunits are related by a 90° rotation. These structural data contribute to a more complete crystallographic picture of large zeolite ZSM-5 crystals, which serve as well-defined model catalysts for zeolite materials. For the first time, the differences in concentration of aluminium within a single crystal were crystallographically mapped, revealing insights into its distribution in zeolite crystallites and the potential impact this will have on catalysis. The synchrotron-based µXRD technique applied allows for creating micrometer-resolved diffraction intensity maps with high angular resolution to reveal the complex structure of various advanced functional materials and important chemical composition gradients as a result of, for example, its structural constituents.

Experimental Section

The experiments were performed at the anomalous scattering beamline ID01 at the European Synchrotron Radiation Facility (ESRF) in Grenoble, France. Laterally resolved diffraction maps of zeolite ZSM-5 crystals were acquired using an X-ray beam (8.5 keV) focused down to a size of 1×2 µm^2. The crystals were scanned by a piezo stage with a step size of 2–3 µm. Diffraction patterns of the studied Bragg reflections were obtained under coplanar diffraction conditions, recorded with a 2D pixel (Maxipix) detector, and further processed by homemade Matlab routines. For details on the µXRD setup, data processing, and zeolite ZSM-5 crystal synthesis, see the Supporting Information.

Received: July 22, 2013
Revised: September 15, 2013
Published online: October 15, 2013

Keywords: aluminium zoning · crystal structures · heterogeneous catalysis · X-ray diffraction · zeolites

[1] a) *Zeolites and Catalysis: Synthesis, Reactions and Applications, Vol. 2* (Eds.: J. Čejka, A. Corma, S. Zones), Wiley-VCH, Weinheim, **2010**; b) *Handbook of Heterogeneous Catalysis*,

Vol. 6 (Eds.: G. Ertl, H. Knözinger, F. Schüth, J. Weitkamp), Wiley-VCH, Weinheim, **2008**.
[2] A. Corma, *Chem. Rev.* **1995**, *95*, 559.
[3] C. S. Lee, T. J. Park, *Appl. Catal. A* **1993**, *96*, 151.
[4] R. J. Quam, L. A. Green, S. A. Tabak, F. J. Krambeck, *Ind. Eng. Chem. Res.* **1988**, *27*, 565.
[5] a) M. Stöcker, *Microporous Mesoporous Mater.* **1999**, *29*, 3; b) U. Olsbye, S. Svelle, P. Beato, T. V. W. Janssens, S. Bordiga, K. P. Lillerud, *Angew. Chem.* **2012**, *124*, 5910; *Angew. Chem. Int. Ed.* **2012**, *51*, 5810.
[6] a) J. C. Groen, L. A. A. Peffer, J. A. Moulijn, J. Pérez-Ramírez, *Chem. Eur. J.* **2005**, *11*, 4983; b) B. M. Weckhuysen, *Angew. Chem.* **2009**, *121*, 5008; *Angew. Chem. Int. Ed.* **2009**, *48*, 4910; c) S. Mitchell, N. Michels, K. Kunze, J. Pérez-Ramírez, *Nat. Chem.* **2012**, *4*, 825; d) I. L. C. Buurmans, B. M. Weckhuysen, *Nat. Chem.* **2012**, *4*, 873.
[7] a) D. Hay, H. Jaeger, K. Wilshier, *Zeolites* **1990**, *10*, 571; b) J. R. Agger, N. Hanif, C. S. Cundy, A. P. Wade, S. Dennison, P. A. Rawlinson, M. W. Anderson, *J. Am. Chem. Soc.* **2003**, *125*, 830; c) E. Stavitski, M. R. Drury, D. A. M. de Winter, M. H. F. Kox, B. M. Weckhuysen, *Angew. Chem.* **2008**, *120*, 5719; *Angew. Chem. Int. Ed.* **2008**, *47*, 5637; d) M. B. J. Roeffaers, R. Ameloot, A.-J. Bons, W. Mortier, G. De Cremer, R. de Kloe, J. Hofkens, D. E. De Vos, B. F. Sels, *J. Am. Chem. Soc.* **2008**, *130*, 13516; e) L. Karwacki et al., *Nat. Mater.* **2009**, *8*, 959 (see the Supporting Information).
[8] a) M. B. J. Roeffaers, B. F. Sels, H. Uji-i, B. Blanpain, P. A. Jacobs, F. C. De Schryver, J. Hofkens, D. E. De Vos, *Angew. Chem.* **2007**, *119*, 1736; *Angew. Chem. Int. Ed.* **2007**, *46*, 1706; b) E. Stavitski, M. H. F. Kox, B. M. Weckhuysen, *Chem. Eur. J.* **2007**, *13*, 7057.
[9] a) O. Geier, S. Vasenkov, E. Lehmann, J. Kärger, U. Schemmert, R. A. Rakoczy, J. Weitkamp, *J. Phys. Chem. B* **2001**, *105*, 10217; b) P. Kortunov, S. Vasenkov, C. Chmelik, J. Kärger, D. M. Ruthven, J. Wloch, *Chem. Mater.* **2004**, *16*, 3552; c) D. Tzoulaki, L. Heinke, W. Schmidt, U. Wilczok, J. Kärger, *Angew. Chem.* **2008**, *120*, 4018; *Angew. Chem. Int. Ed.* **2008**, *47*, 3954; C. Chmelik, J. Kärger, *Chem. Soc. Rev.* **2010**, *39*, 4543.
[10] a) C. Weidenthaler, R. X. Fischer, R. D. Shannon, O. Medenbach, *J. Phys. Chem.* **1994**, *98*, 12687; b) L. Karwacki, E. Stavitski, M. H. F. Kox, J. Kornatowski, B. M. Weckhuysen, *Angew. Chem.* **2007**, *119*, 7366; *Angew. Chem. Int. Ed.* **2007**, *46*, 7228; c) M. B. J. Roeffaers et al., *J. Am. Chem. Soc.* **2008**, *130*, 5763 (see the Supporting Information); d) M. H. F. Kox, E. Stavitski, J. C. Groen, J. Pérez-Ramírez, F. Kapteijn, B. M. Weckhuysen, *Chem. Eur. J.* **2008**, *14*, 1718; e) G. De Cremer, B. F. Sels, D. E. De Vos, J. Hofkens, M. B. J. Roeffaers, *Chem. Soc. Rev.* **2010**, *39*, 4543; R. A. Schoonheydt, *Chem. Soc. Rev.* **2010**, *39*, 5051.
[11] a) M. H. F. Kox, K. F. Domke, J. P. R. Day, G. Rago, E. Stavitski, M. Bonn, B. M. Weckhuysen, *Angew. Chem.* **2009**, *121*, 9152; *Angew. Chem. Int. Ed.* **2009**, *48*, 8990; b) K. F. Domke, J. P. R. Day, G. Rago, T. A. Riemer, M. H. F. Kox, B. M. Weckhuysen, M. Bonn, *Angew. Chem.* **2012**, *124*, 1371; *Angew. Chem. Int. Ed.* **2012**, *51*, 1343.
[12] a) E. Stavitski, M. H. F. Kox, I. Swart, F. M. F. de Groot, B. M. Weckhuysen, *Angew. Chem.* **2008**, *120*, 3599; *Angew. Chem. Int. Ed.* **2008**, *47*, 3543; b) E. Stavitski, B. M. Weckhuysen, *Chem. Soc. Rev.* **2010**, *39*, 4615.
[13] G. M. Pennock, A. Barnhoorn, A. J. Bons, M. J. Drury, *J. Mater. Sci. Lett.* **2001**, *20*, 1099.
[14] a) E. L. Wu, S. L. Lawton, D. H. Olson, A. C. Rohrman, G. T. Kokotailo, *J. Phys. Chem.* **1979**, *83*, 2777; b) H. van Koningsveld, J. C. Jansen, H. van Bekkum, *Zeolites* **1990**, *10*, 235.
[15] a) C. Mocuta, J. Stangl, K. Mundboth, T. H. Metzger, G. Bauer, I. A. Vartanyants, M. Schmidbauer, T. Boeck, *Phys. Rev. B* **2008**, *77*, 245425; b) A. M. Beale, S. D. Jacques, B. M. Weckhuysen, *Chem. Soc. Rev.* **2010**, *39*, 4656; c) J. Ruiz-Martínez, A. M. Beale, U. Deka, M. G. O'Brien, P. D. Quinn, J. F. W. Mosselmans, B. M. Weckhuysen, *Angew. Chem.* **2013**, *125*, 6099; *Angew. Chem. Int. Ed.* **2013**, *52*, 5983; d) J. D. Grunwaldt, C. G. Schroer, *Chem. Soc. Rev.* **2010**, *39*, 4543; S. Bordiga, E. Groppo, J. A. van Bokhoven, C. Lamberti, *Chem. Rev.* **2013**, *113*, 1736; e) N. Tamura, A. A. MacDowell, R. Spolenak, B. C. Valek, J. C. Bravman, W. L. Brown, R. S. Celestre, H. A. Padmore, B. W. Batterman, J. R. Patel, *J. Synchrotron Radiat.* **2003**, *10*, 137; f) M. Müller, M. Burghammer, D. Flot, C. Riekel, C. Morawe, B. Murphy, A. Cedola, *J. Appl. Crystallogr.* **2000**, *33*, 1231; g) P. Sciau, P. Goudeau, N. Tamura, E. Dooryhee, *Appl. Phys. A* **2006**, *83*, 219.
[16] a) D. Mores, J. Kornatowski, U. Olsbye, B. M. Weckhuysen, *Chem. Eur. J.* **2011**, *17*, 2874; b) J. P. Hofmann, D. Mores, L. R. Aramburo, S. Teketel, M. Rohnke, J. Janek, U. Olsbye, B. M. Weckhuysen, *Chem. Eur. J.* **2013**, *19*, 8533.
[17] J. B. Jones, *Acta Crystallogr. Sect. B* **1968**, *24*, 355.
[18] a) K. Chao, J. Chern, *Zeolites* **1988**, *8*, 82; b) R. Althoff, B. Schulz-Dobrick, F. Schüth, K. Unger, *Microporous Mater.* **1993**, *1*, 207; c) N. Danilina, F. Krumeich, S. A. Castelanelli, J. A. van Bokhoven, *J. Phys. Chem. C* **2010**, *114*, 6640.
[19] R. von Ballmoos, W. M. Meier, *Nature* **1981**, *289*, 782.

